PHYSICAL REVIEW B VOLUME 56, NUMBER 9 1 SEPTEMBER 1997-I

Magnetic ordering of the antiferromagnet Cu_2MnSnS_4 from magnetization and neutron-scattering measurements

T. Fries and Y. Shapira
Department of Physics and Astronomy, Tufts University, Medford, Massachusetts 02155

Fernando Palacio and M. Carmen Morón
Instituto de Ciencia de Materiales de Aragón, CSIC-Universidad de Zaragoza, 5009 Zaragoza, Spain

Garry J. McIntyre
Institut Laue-Langevin, B. P. 156, 38042 Grenoble Cedex 9, France

R. Kershaw and A. Wold
Department of Chemistry, Brown University, Providence, Rhode Island 02912

E. J. McNiff, Jr.
Francis Bitter National Magnet Laboratory, Massachusetts Institute of Technology, Cambridge, Massachusetts 02139

(Received 17 January 1997)

Magnetization and neutron-diffraction measurements were performed on a single crystal of Cu_2MnSnS_4. This quartenary magnetic semiconductor has the stannite structure (derived from the zinc-blende structure which is common to many II-VI dilute magnetic semiconductors), and it orders antiferromagnetically at low temperature. The neutron data for the nuclear structure confirm that the space group is $I\bar{4}2m$. Both the neutron and magnetization data give $T_N = 8.8$ K for the Néel temperature. The neutron data show a collinear antiferromagnetic (AF) structure with a propagation vector $\mathbf{k}=[1/2,0,1/2]$, in agreement with earlier neutron data on a powder. However, the deduced angle θ between the spin axis and the crystallographic c direction is between 6° and 16°, in contrast to the earlier value of 40°. The magnetization curve at $T \ll T_N$ shows the presence of a spin rotation (analogous to a spin flop), which indicates that the spin axis is indeed close to the c direction. The deduced magnetic anisotropy gives an anisotropy field $H_A \cong 2$ kOe. At high magnetic fields the magnetization curve at $T \ll T_N$ shows the transition between the canted (spin-flop) phase and the paramagnetic phase. The transition field, $H = 245.5$ kOe, yields an intersublattice exchange field $H_E = 124$ kOe. The exchange constants deduced from H_E and the Curie-Weiss temperature $\Theta = -25$ K show that the antiferromagnetic interactions are an order of magnitude smaller than in II-VI dilute magnetic semiconductors (DMS's). The much weaker antiferromagnetic interactions are expected from the difference in the crystal structures (stannite versus zinc-blende). A more surprising result is that the exchange constant which controls the AF order below T_N is *not* between Mn ions with the smallest separation. This result contrasts with a prediction made for the related II-VI DMS, according to which the exchange constants decrease rapidly with distance. [S0163-1829(97)04234-3]

I. INTRODUCTION

Dilute magnetic semiconductors (DMS's) have been the subject of active research in the last two decades.[1,2] Much of the work has focused on Mn-based II-VI DMS's with zinc-blende or wurtzite crystal structure. A major limitation of these materials arises from the strong antiferromagnetic (AF) interaction between nearest-neighbor (NN) Mn ions, governed by the NN exchange constant J_1. This J_1 is by far the largest exchange constant. The AF interaction becomes increasingly more important as the Mn concentration x increases, because a larger percentage of the Mn ions become connected by J_1 bonds. As a result, it is difficult to align the Mn spins when x is large, even when magnetic fields H of order 100 kOe are applied at low temperatures. The inability to achieve large magnetizations frustrates attempts to increase the size of magneto-optical effects by increasing x. The strong NN exchange interaction also limits the achievable binding energies for bound magnetic polarons (BMP's) in II-VI DMS.[3]

Quartenary DMS's with the stannite or wurtz-stannite crystal structures were suggested as a way of avoiding large AF exchange interactions.[4,5] Examples of materials having these structures are discussed in Ref. 6. Figure 1 shows the stannite structure of Cu_2MnSnS_4. In many respects there is a strong similarity to the zinc-blende structure, e.g., each cation is tetrahedrally coordinated to four sulfur anions. However, unlike zinc-blende materials there are three types of cations, with three different valences. The unit cell is therefore doubled in the c direction. A crucial point is that the three types of cations occupy *ordered positions* in the structure. The Mn ions form a body-centered tetragonal lattice. The minimum distance between two Mn cations is then the lattice constant a, which is larger than the NN distance $a/\sqrt{2}$ in the corresponding zinc-blende structure. As a consequence, the exchange interaction which corresponds to the NN exchange constant J_1 in II-VI DMS's is absent. The re-

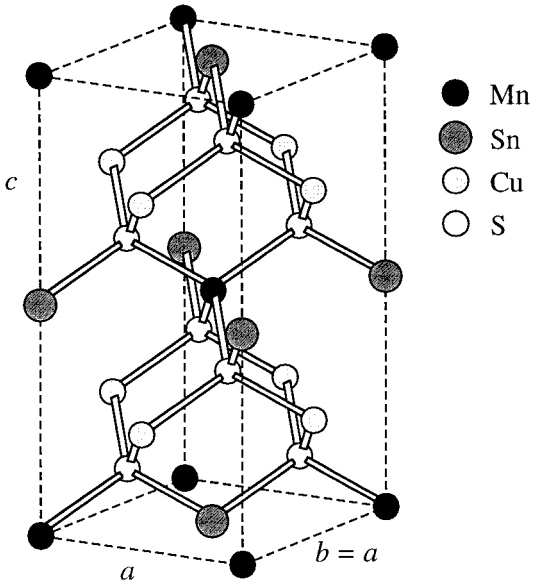

FIG. 1. The stannite structure of Cu_2MnSnS_4.

maining exchange interactions are expected to be smaller by at least one order of magnitude.[7] The absence of J_1 should greatly reduce the overall AF exchange interactions in stannite DMS. A similar reduction of the AF interactions is expected for DMS with the wurtzite-stannite structure. The latter prediction was already confirmed in Cu_2MnGeS_4, which has the wurtz-stannite structure.[8]

Previous works on Cu_2MnSnS_4 include the determination of the crystal structure and lattice parameters, and the observation that the material is an antiferromagnet with a Néel temperature T_N below 20 K (the exact value was not determined).[6,9] Early neutron-diffraction data on a powder[10] suggested that the AF structure is collinear, with a propagation vector $\mathbf{k}=[1/2,0,1/2]$, and with the spin axis 40° from the crystallographic c direction.

In the present paper we present neutron-diffraction and magnetization data on a single crystal of Cu_2MnSnS_4. The neutron data confirm many of the earlier findings,[10] but show that the spin axis is much closer to the c direction. This conclusion is strongly supported by the magnetization data. Both neutron and magnetic-susceptibility data give a precise value for T_N. The magnetization data show the characteristic phase transitions of a collinear antiferromagnet: the analog of the spin-flop transition, and the order-disorder transition from the canted phase to the paramagnetic phase. The phase transitions give both the magnetic anisotropy K and the intersublattice exchange field H_E. The data confirm the prediction that the AF interactions in the stannite structure are much weaker than in the zinc-blende structure. A related study of the magnetic properties of BMP's in $Cu_2Mn_{0.9}Zn_{0.1}SnS_4$ will be published separately.[11]

II. EXPERIMENT

The single crystal of Cu_2MnSnS_4, with dimensions of about $3\times2\times2$ mm, was obtained from a boule grown by the Bridgman method. The crystal had high resistivity at room temperature, and showed none of the magnetic features of BMP's at low temperatures.[11] The high resistivity and absence of BMP effects indicate that the concentrations of acceptors and/or donors were too low to affect the magnetic behavior.

The neutron-diffraction experiments were performed on the D10 diffractometer of the Institut Laue Langevin, Grenoble (France), in the standard four-circle configuration. The offset Eulerian cradle of this diffractometer is equipped with a helium-flow cryostat operating between 1.6 and 300 K with full four-circle accessibility. All measurements were performed at a constant wavelength of 1.2593 Å obtained from the (200) planes of a copper monochromator and calibrated using a ruby single crystal. The half-wavelength contamination in the incident beam in this configuration is less than 2×10^{-4}. Reflection data corresponding to the nuclear lattice were collected first. A total of 701 reflections were collected at 15.2 K, a temperature which is above but close to the antiferromagnetic transition. Data for analysis of the ordered magnetic phase were taken at 2 K. The temperature dependence of a few selected magnetic reflections was followed in the range from 2 to 12 K. Finally, data from 15 unique reflections were collected at room temperature. The data were analyzed using programs based on the Cambridge Crystallographic Subroutine Library.[12] All data were corrected for background by the minimum $\sigma(I)/I$ method,[13] and for absorption using a calculated absorption coefficient of 0.0109 mm^{-1}. The transmission factors ranged from 0.975 to 0.998

Magnetization data were obtained with two different magnetometers. Measurements at relatively low magnetic fields, $H\leqslant55$ kOe, were performed with a SQUID magnetometer system manufactured by Quantum Design Inc. This system was operated at temperatures $1.9<T<300$ K. Data at higher fields, up to 300 kOe, were obtained at 1.4 K using a vibrating sample magnetometer which was adapted for use in a hybrid magnet. (A hybrid magnet consists of a Bitter magnet inside a wide-bore superconducting magnet.) Prior to performing the magnetization measurements the sample was oriented using x rays. The angle between the c axis of the sample and the magnetic field **H** was controlled to better than 4°.

III. NEUTRON-DIFFRACTION RESULTS

A. Nuclear structure

The reported tetragonal stannite structure of Cu_2MnSnS_4 results from a doubling of the zinc-blende lattice parameters along the c crystallographic direction. The resulting space group symmetry at room temperature was determined to be $I\bar{4}2m$ (Ref. 9). In the present work, structural refinement of the atomic positions at 300 K was performed on a limited set of 15 unique reflections. Although the data were limited, the refined crystallographic parameters and atomic positions are in acceptable agreement with the previous determination.[9] The results at 300 K are listed in Table I. The origin of the unit cell has been located at the Mn position.

The crystallographic parameters and atomic positions at 15.2 K, from refinement in space group $I\bar{4}2m$ against data collected at that temperature, are given in Table II. These results show very good agreement with the proposed structural model. The space group $I\bar{4}$ which often describes struc-

TABLE I. Atomic coordinates and thermal parameters (temperature factors) B for Cu_2MnSnS_4 at 300 K. (Number of observations: 15 unique reflections. Number of variables: 7. Correlations: less than 70%. Agreement factors: $wR=0.008$, $\chi^2=3.1$.) The unit-cell parameters are $a=5.517(2)$ Å and $c=10.806(8)$ Å.

Element	X	Y	Z	B (Å^2)
Cu	0	1/2	1/4	1.7(2)
Mn	0	0	0	2.6(6)
Sn	0	0	1/2	0.6(3)
S	0.252(2)	X	0.1314(9)	1.2(5)

tures derived from the zinc blende was also considered as a possibility. The only practical difference between a structural description of Cu_2MnSnS_4 in $I42m$ and in $I4$ is that the positions of the S atoms depend on three parameters (X,Y,Z) in $I4$ instead of two (X,X,Z) in $I42m$. In fact, $I4$ is a subgroup of $I42m$. The refinement in the space group $I4$ yielded an agreement factor $wR=0.025$ and atomic positions for the S atoms $[X=0.2521(1)$, $Y=0.2521(1)$, and $Z=0.132\,95(6)]$ matching within experimental uncertainty the positions refined in the $I42m$ space group. The space group $I4$ was then discarded on the basis of equal values for the X and Y coordinates of the S atom and the poorer agreement factor. Thus, the possibility of minor structural changes in the cooling process, which reduce the symmetry of the compound, can be excluded.

B. Magnetic structure

As the temperature is decreased below approximately 9 K additional diffraction peaks start to develop in rows parallel to half-integer values of reciprocal space axes, while the intensities of the nuclear reflections remain unchanged. Figure 2 shows the positions of the nuclear and magnetic reflections in the $\boldsymbol{a}^*\boldsymbol{0}\boldsymbol{c}^*$ plane of the reciprocal space. Scans along the main symmetry directions revealed equal intensities for magnetic reflections from four equivalent **k**-propagation vectors: [1/2,0,1/2], [−1/2,0,1/2], [0,1/2,1/2], and [0,−1/2,1/2]. This situation can correspond either to a collinear structure with propagation vector $\mathbf{k}=[1/2,0,1/2]$ and equal populations of the four K domains, or to a structure with multi-**k** ordering.

TABLE II. Atomic coordinates and thermal parameters for Cu_2MnSnS_4 at 15.2 K. (Number of observations: 199 unique reflections. Number of variables: 13. Correlations: less than 70%. Agreement factors: $wR=0.0155$, $\chi^2=3.38$. Thermal parameters relate to the expression $\exp[(-1/4)(B_{11}h^2a^{*2}+B_{22}k^2b^{*2}+B_{33}l^2c^{*2}+2B_{12}ha^*kb^*+2B_{23}kb^*lc^*+2B_{13}ha^*lc^*)]$. By symmetry $B_{22}=B_{11}$ for all atoms and $B_{13}=B_{23}=B_{12}=0$ for Cu, Mn, and Sn. In the case of S atoms B_{13}, B_{23}, and B_{12} refine to 0 within the standard deviation.) The unit-cell parameters are $a=5.514(1)$ Å and $c=10.789(4)$ Å.

Element	X	Y	Z	B_{11}(Å^2)	B_{33} (Å^2)
Cu	0	1/2	1/4	0.220(9)	0.262(12)
Mn	0	0	0	0.340(20)	0.279(31)
Sn	0	0	1/2	0.084(12)	0.126(17)
S	0.252 06(10)	X	0.132 95(8)	0.287(21)	0.252(25)

To distinguish between the two cases in a neutron-diffraction experiment it would be necessary to apply a small external perturbation, such as a magnetic field. The perturbation would modify the balance among the domains in the case of the single-**k** structure but would not change the multi-**k** structure. Such an experiment was not performed. However, the susceptibility and magnetization measurements reported below are consistent with a collinear structure and exclude multi-**k** ordering. The propagation vector $\mathbf{k}=[1/2,0,1/2]$ has also been suggested in an earlier magnetic-structure determination from a powder sample.[10] The resulting magnetic unit cell doubles the nuclear one along the a and c crystallographic directions.

The only magnetic atoms in the unit cell are the Mn^{2+} ions, since the Cu ions are in the valence state +1 with a closed $3d$ shell. The wave vector $\mathbf{k}=[1/2,0,1/2]$, i.e., $\mathbf{k}=0.5\boldsymbol{a}^*+0.5\boldsymbol{c}^*=(0.5/a)\hat{\boldsymbol{a}}+(0.5/c)\hat{\boldsymbol{c}}$, means that the direction of the magnetic moment $\boldsymbol{m}$ of a Mn^{2+} ion located at $\boldsymbol{r}$ is given by

$$\mathbf{m}(\mathbf{r})=\mathbf{m}(0)\,\exp(-2\pi i\mathbf{k}\cdot\mathbf{r}). \tag{1}$$

The resulting magnetic structure is represented in Fig. 3.

Values for the magnetic moment of the Mn ion, $m=4.28(4)\mu_B$, and for the angle that the moment makes with the c crystallographic direction, $\theta=16(2)°$, have been ob-

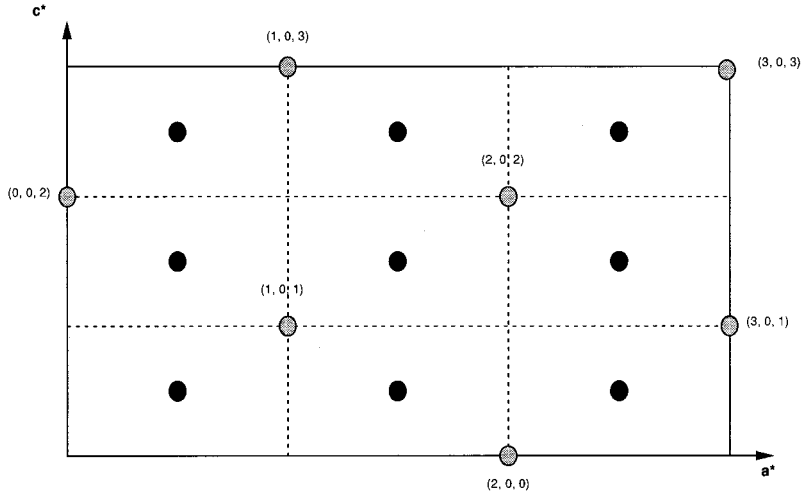

FIG. 2. Reciprocal-space plane showing the scattering points associated with nuclear reflections (shaded circles) and magnetic reflections (filled circles).

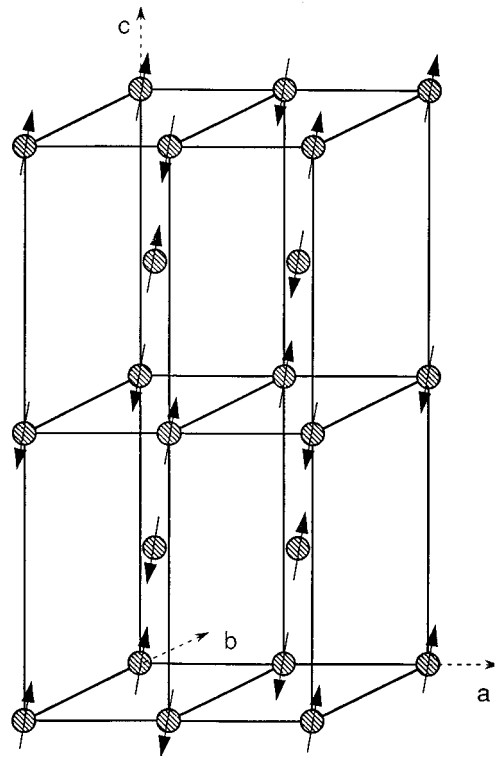

FIG. 3. Orientations of the moments in the magnetic unit cell of Cu_2MnSnS_4 for $\mathbf{k}=[1/2,0,1/2]$.

tained from a fit to 198 independent magnetic reflections. The program MAGLSQ of CCSL (Ref. 12) was used in this fit with the nuclear parameters fixed to those determined at 15.2 K. The fitting agreement factors were $wR=0.10$ and $\chi^2=6.6$. The value of m is somewhat lower than the theoretically expected value of $5\mu_B$ (for a spin 5/2 with $g=2$), and is also lower than the value $m=4.7\mu_B$ obtained from the magnetization data reported below. The difference should be attributed to small electronic transfer to neighboring sulfur atoms due to covalence effects.

The value for the angle θ obtained from the fitting is, in fact, less precise than the uncertainty given by the quoted standard deviation. When some low-intensity reflections are excluded from the fit, the value of the moment m remains unaffected but θ can move to any value between 6° and 16°. The value 16° which was quoted above (on the basis of *all* the measured magnetic reflections) is therefore viewed as an upper limit. This upper limit is still substantially below the value $\theta=40°$ obtained from the early neutron-diffraction data on a powder.[10] Because θ is not zero, the magnetic moment has a component in the basal plane (ab plane or xy plane). In the present experiments, symmetry constraints excluded the possibility of determining the orientation of this component in the basal plane.

The orientation of the spin axis does not agree with calculations of the dipole-dipole anisotropy. The dipole-dipole energy for a domain with $\mathbf{k}=[1/2,0,1/2]$ is minimum when the spin axis is along the y direction, i.e., $\theta=90°$. Evidently, there are other sources for the anisotropy in this antiferromagnet. As discussed later, the net magnetic anisotropy is quite small.

The temperature dependence of the intensities of some selected magnetic reflections has been followed. Figure 4 shows the integrated intensities as a function of temperature for the (0,1/2,1/2), (1/2,1,1/2), (−1/2,0,−1/2), and (−3/2,0,1/2) reflections. The intensities of all these reflections, which are purely magnetic, show a sharp rise at the Néel temperature $T_N=8.8$ K.

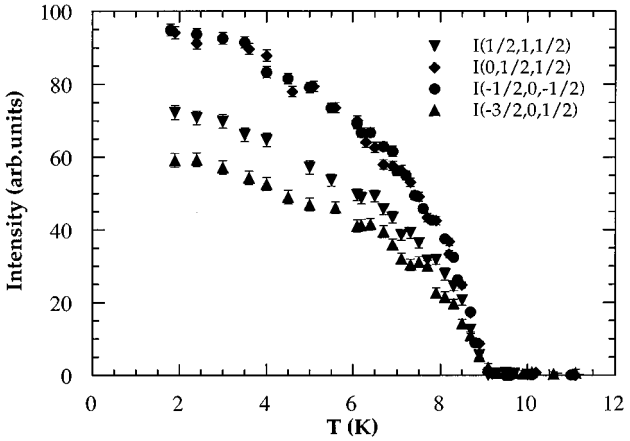

FIG. 4. Temperature dependence of four selected magnetic reflections.

IV. MAGNETIZATION

A. Low-field susceptibility

The susceptibility $\chi=M/H$ was measured with the SQUID magnetometer system. Data below 20 K were taken at $H=1$ kOe with **H** parallel and perpendicular to the c axis. The results are shown in Fig. 5. The overall behavior agrees with the AF structure deduced from the neutron results, i.e., a collinear AF structure with spin axis close to the c direction. A well-known example of an ideal collinear AF is MnF_2, in which there is a single easy axis parallel to the tetragonal crystallographic direction.[14] The susceptibilities in Fig. 5, for the two field directions, resemble those in MnF_2 but with two exceptions. First, unlike MnF_2, the susceptibility for $\mathbf{H}\|\boldsymbol{c}$ does not approach zero as $T\rightarrow 0$. This difference is partially (but not fully) explained by the finite angle θ between the c direction and the spin axis in each of the four K domains of Cu_2MnSnS_4. The second difference, compared

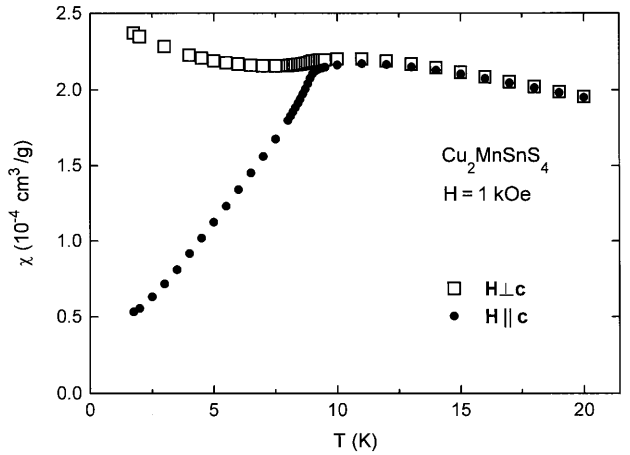

FIG. 5. Temperature dependence of the magnetic susceptibility χ (per unit mass) for **H** parallel and perpendicular to the c axis.

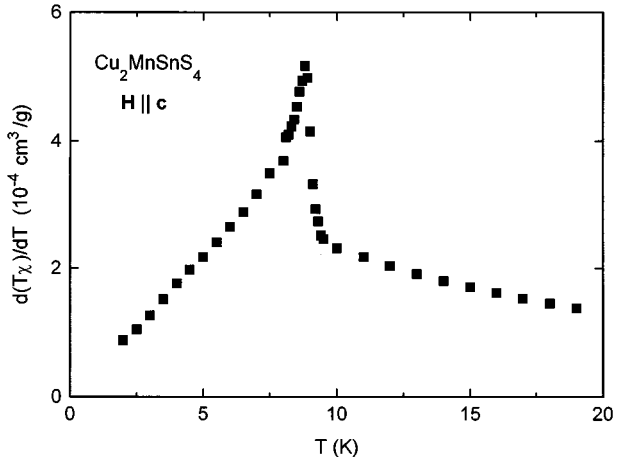

FIG. 6. The derivative $d(T\chi)/dT$ for $\mathbf{H}\|\boldsymbol{c}$. These results were obtained numerically from the data in Fig. 5.

to MnF_2, is that the susceptibility for $\mathbf{H}\perp\boldsymbol{c}$ exhibits a small rise below T_N. Note that at $T>10$ K, where the Cu_2MnSnS_4 is in the paramagnetic phase, the susceptibility is practically independent of the direction of $\boldsymbol{H}$. This feature is typical for a low-anisotropy antiferromagnet.

Figure 6 shows the derivative $d(T\chi)/dT$ for $\mathbf{H}\|\boldsymbol{c}$. These results were obtained numerically from the data in Fig. 5. The λ anomaly exhibited by $d(T\chi)/dT$ should resemble the anomaly in the specific heat.[15] From the location of the peak in Fig. 6 the Néel temperature is $T_N=8.8\pm0.1$ K, in agreement with the neutron data. The value of T_N is only a few percent higher than for Cu_2MnGeS_4.[8]

Susceptibility data for $T\geqslant50$ K and for $T\geqslant100$ K were taken in fields of 25 and 50 kOe, respectively. These fields are ''weak'' in the sense that $mH\ll k_BT$, where m is the magnetic moment of a Mn^{2+} ion and k_B is the Boltzmann constant. The data for $1/\chi$ are shown in Fig. 7. They have been corrected for the lattice diamagnetism assuming a lattice susceptibility $\chi_d=-3\times10^{-7}$ emu/g, typical for this type of material.[8] Because the lattice correction is relatively small, the uncertainty in χ_d is unimportant. Fits of the data

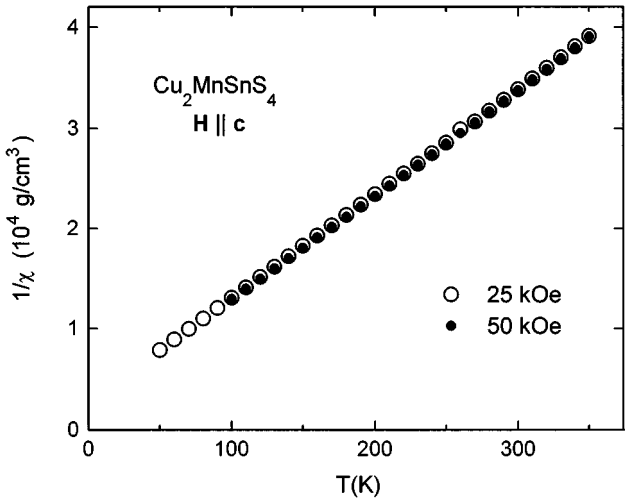

FIG. 7. Temperature dependence of the inverse susceptibility $1/\chi$ per unit mass. These data have been corrected for the lattice diamagnetism.

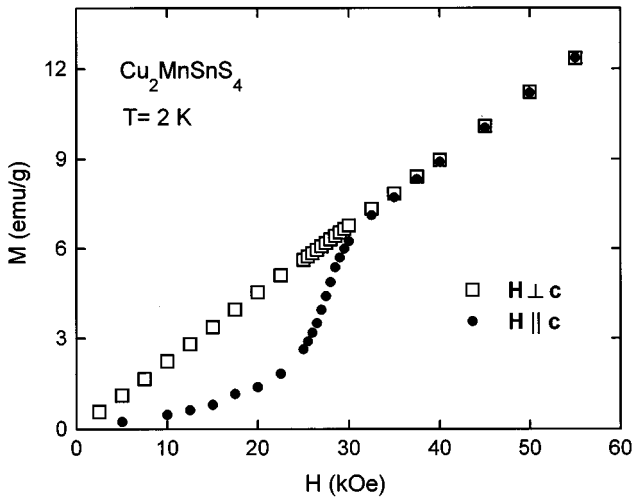

FIG. 8. Field dependence of the magnetization at 2 K, for **H** parallel and perpendicular to the c axis.

for χ vs T to the Curie-Weiss law gave a Curie constant $C=(0.96\pm0.02)\times10^{-2}$ cm^3 K/g and a Curie-Weiss temperature $\Theta=-(25\pm2)$ K. The quoted uncertainties include variations introduced by changing the temperature range in the fit, e.g., using only data above 150 K. If one assumes that each Mn^{2+} ion has a spin $S=5/2$ and a g factor of 2.00, the theoretical value of C is 1.02×10^{-2} cm^3 K/g, i.e., 6% above the experimental value. Of greater significance from our perspective is the value of Θ. As discussed later, it indicates that the AF interactions in this stannite material have been reduced by more than an order of magnitude relative to a comparable zinc-blende material.

B. Spin rotation

The spin-flop transition in easy axis antiferromagnets is well known.[14,16–18] This first-order transition occurs when **H** is parallel, or nearly parallel, to the spin axis. At the transition the sublattice magnetizations $\mathbf{M}_1$ and $\mathbf{M}_2$ rotate abruptly. The staggered magnetization $\boldsymbol{L}=\mathbf{M}_1-\mathbf{M}_2$ then rotates into a direction perpendicular to **H**. The transition manifests itself as an abrupt increase in the total magnetization $\mathbf{M}=\mathbf{M}_1+\mathbf{M}_2$. The magnetic phase above the transition is known as the ''spin-flop'' phase, or as the ''canted'' phase (because $\mathbf{M}_1$ and $\mathbf{M}_2$ are canted relative to each other in this phase).

When the angle ϕ between **H** and the spin axis exceeds a certain (small) value, the first-order transition disappears.[19] Instead, there is a gradual rotation of $\mathbf{M}_1$ and $\mathbf{M}_2$. Experimentally, the gradual rotation appears as a smeared spin-flop ''transition'' (see, e.g., Figs. 2 and 3 in Ref. 14). The smearing increases with ϕ. In the present material the spin axis makes a finite angle, $\theta\leqslant16°$, with the c direction. Therefore, a smeared spin-flop transition is expected when **H** is parallel to c.

Magnetization data at 2 K, for **H** parallel and perpendicular to the c direction, are shown in Fig. 8. These data were obtained with the SQUID magnetometer. The results for $\mathbf{H}\|\boldsymbol{c}$ show the characteristic signature of spin rotation (smeared spin-flop transition). The center of the ''transition,'' where dM/dH is maximum, is at 28 kOe. Unlike the results for

$\mathbf{H}\|\boldsymbol{c}$, the magnetization for $\mathbf{H}\perp\boldsymbol{c}$ is nearly proportional to H. For $H\geqslant 35$ kOe the magnetizations for the two field directions are equal. Such equal magnetizations are expected at high fields because for both field configurations ($\mathbf{H}\|\boldsymbol{c}$ and $\mathbf{H}\perp\boldsymbol{c}$) the staggered magnetization $\mathbf{L}$ is perpendicular to $\mathbf{H}$. The susceptibility for both field directions is then the perpendicular susceptibility $\chi_\perp$.

The magnetization curves in Fig. 8 can be used to obtain a certain anisotropy energy. At zero field, the free energy G_{AF} for the actual spin orientation (with $\mathbf{L}$ making a small angle θ with the c direction) is lower than the free energy G_{SF} for the spin-flop configuration with $\mathbf{L}\perp\boldsymbol{c}$. The difference $K=\Delta G$ is an anisotropy energy. It is given by the area between the two magnetization curves in Fig. 8.[16] Numerical integration gives $K=6.1\times10^4$ erg/g. Because the data of Fig. 8 were taken at $T/T_N<1/4$, this value for K should not differ appreciably from that at $T=0$. By analogy to the case of an easy-axis antiferromagnet, we define an anisotropy field $H_A=K/M_S$, where M_S is the sublattice magnetization. This gives $H_A=2$ kOe, which is a fairly low anisotropy field, consistent with the fact that Mn^{2+} is an S-state ion. The field H_A is much smaller than the intersublattice exchange field H_E discussed below.

C. Canted-to-paramagnetic transition

At sufficiently high magnetic fields there is an order-disorder transition from the canted phase into the paramagnetic phase.[16–18] The relevant order parameter is the staggered magnetization, which is finite in the canted (ordered) phase but vanishes in the paramagnetic (disordered) phase. In mean-field theory the canted-to-paramagnetic transition is accompanied by a sharp drop in the differential susceptibility dM/dH. More sophisticated treatments (such as spin-wave theory and modern theory of critical points) lead to a λ singularity in dM/dH, as discussed in Ref. 18. In three-dimensional materials the λ singularity becomes small at low temperatures, $T\ll T_N$. The main feature at the transition is then the large drop in dM/dH. When the direction of $\mathbf{H}$ is close to the zero-field spin axis, the transition field H_c is given by[18]

$$H_c=2H_E-H_A, \tag{2}$$

where H_E is the *intersublattice* exchange field. The intrasublattice exchange field does not affect H_c.[17] In the present case the anisotropy field H_A is very small compared to $2H_E$, so that H_c is controlled by H_E. Although all quantities in Eq. (2) are temperature dependent, the changes when $T/T_N\ll 1$ are small.

Figure 9(a) shows the magnetization curve at 1.4 K in fields up to 300 kOe. These data were obtained in a hybrid magnet using a vibrating sample magnetometer. The relatively fast rise of the magnetization M near 28 kOe corresponds to the spin rotation in Fig. 8. Following this rise the slope dM/dH remains nearly constant until the canted-to-paramagnetic transition takes place at high fields. Near 300 kOe the magnetization is practically saturated, at a value of 61 ± 1 emu/g. The theoretical saturation value, assuming $S=5/2$ and $g=2.00$ for the Mn^{2+} ion, is 65 emu/g.

The derivative dM/dH, obtained numerically from the magnetization curve in Fig. 9(a), is shown in Fig. 9(b). The spin rotation near 28 kOe appears as a large peak. The canted-to-paramagnetic transition appears as a small λ peak followed by a large drop. The position of the λ peak, at 245.5 ± 3 kOe, is taken as the transition field. Using Eq. (2), with $H_A=2$ kOe, one then obtains $H_E=124$ kOe for the intersublattice exchange field. Because this value was obtained at $T/T_N=0.16$, it should be close to $H_E(0)$ at $T=0$. The ratio $\alpha=H_A/H_E=1.6\times10^{-2}$ is quite low. Both the values of H_E and H_A in Cu_2MnSnS_4 are comparable to those in Cu_2MnGeS_4.[8]

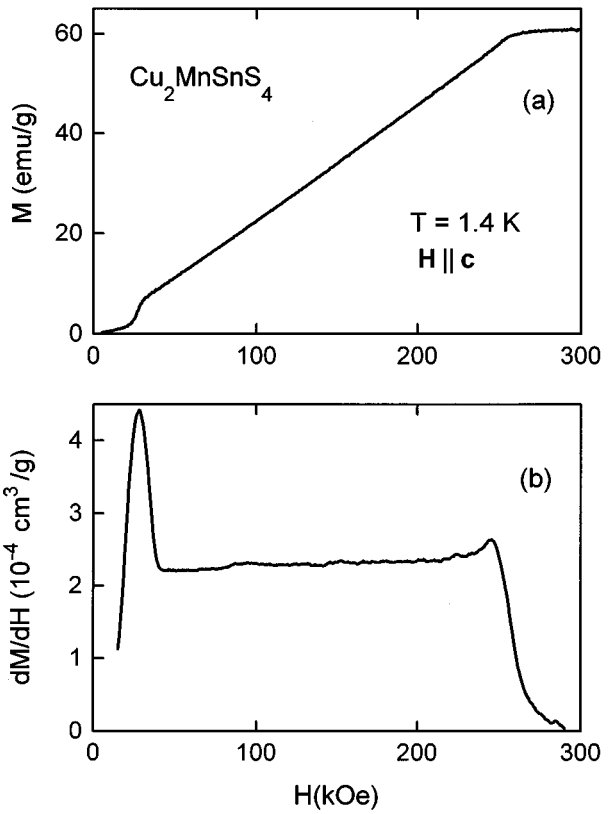

FIG. 9. (a) Magnetization curve at 1.4 K, for $\mathbf{H}\|\boldsymbol{c}$. (b) Field dependence of the derivative dM/dH obtained numerically from the results in (a).

V. EXCHANGE INTERACTIONS

To discuss the exchange interactions in Cu_2MnSnS_4 we introduce the notation in Fig. 10 for the exchange constants J_i. This notation is purposely based on the convention *for zinc-blende materials*. The exchange constant J_1 in the zinc-blende structure is missing in Fig. 10. The reason is that the minimum separation between two Mn ions in the stannite structure is the lattice constant a, which corresponds to the exchange constant J_2 in the zinc-blende structure. The next two exchange constants, J_3 and J_4, are for Mn ions separated by $a\sqrt{3/2}$ and $a\sqrt{2}$, respectively, as in the zinc-blende structure. We assume that other exchange constants, for larger separations, can be neglected.

The magnetization data indicate that the AF exchange interactions in Cu_2MnSnS_4 are considerably weaker than in a similar material with the zinc-blende structure. The strongest evidence for this conclusion is the Curie-Weiss temperature

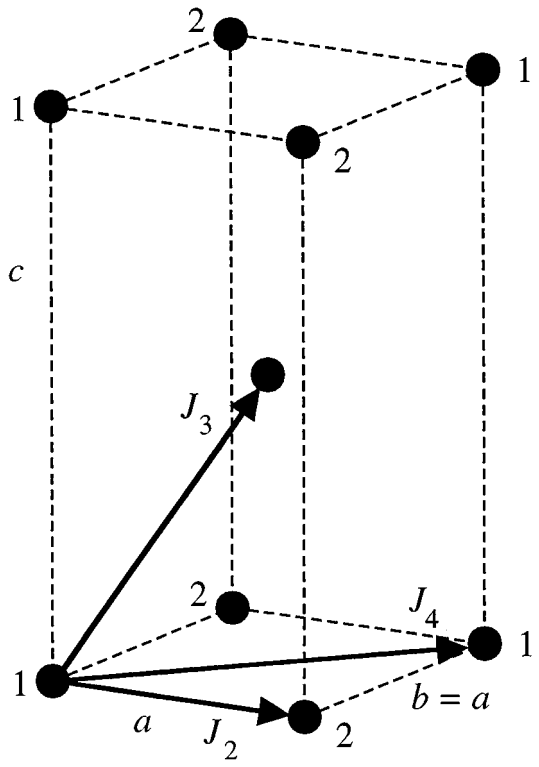

FIG. 10. Notation for the exchange constants J_i in Cu_2MnSnS_4. This notation is based on the convention for the zinc-blende structure. The closest neighbors in the stannite structure of Cu_2MnSnS_4 are separated by a distance which corresponds to the second neighbors in the zinc-blende structure. These closest neighbors are therefore coupled by J_2. The exchange constant J_1, for spins separated by $a/\sqrt{2}$, does not exist in the stannite structure.

Θ, which is related to the exchange constants as

$$k_B\Theta=[2S(S+1)/3]\sum z_iJ_i. \tag{3}$$

Here, z_i is the number of neighbors coupled to a given Mn ion by the exchange constant J_i. In the present material $\Theta=-25$ K. The corresponding II-VI antiferromagnet is β-MnS which has two structures, zinc-blende and wurtzite. The Θ's for these structures are -982 and -932 K, respectively.[20] The main reason why Θ for Cu_2MnSnS_4 is so much lower is that J_1 is absent. A second reason is that there are fewer neighbors connected by J_2, J_3, and J_4 exchange bonds ($z_2=4$, $z_3=8$, $z_4=4$ for stannite, compared to $z_2=6$, $z_3=24$, $z_4=12$ for zinc blende).

Another indication that the exchange interactions in Cu_2MnSnS_4 are considerably weaker than in II-VI DMS is the lower magnetic field required to saturate the magnetization at low temperatures. Figure 9(a) shows that complete saturation is achieved at 300 kOe. In a comparable II-VI DMS, $Cd_{1-x}Mn_xTe$ with $x=0.25$, the low-temperature value of M at 300 kOe is only a third of its saturation value.[21]

A much more surprising result is derived from the AF structure obtained by neutron diffraction. The structure in Fig. 3 implies that the exchange constant J_4, between Mn ions separated by $a\sqrt{2}$, controls the AF order. All four J_4 exchange bonds are satisfied in this structure. In contrast, only two of the four J_2 exchanged bonds (along the $\pm a$ directions) are satisfied but the other two J_2 bonds (along the $\pm b$ directions) are frustrated. On the basis of the current theory for zinc-blende DMS (Refs. 7, 22, and 23) one might have expected that J_2 is one or two orders of magnitude larger than J_4. If the AF order were governed by J_2, all four J_2 bonds would have been satisfied and the four J_4 bonds would have been frustrated (i.e., the four Mn spins whose distance from an ''up'' spin is the lattice constant a would have had their spins ''down''). Comparing the actual AF order to hypothetical AF order with $\mathbf{k}=[1/2,1/2,0]$ in which all J_2 interactions are satisfied, one concludes that $|J_4|$ must be larger than $|J_2/2|$. This conclusion was actually reached earlier,[10] before extensive investigations of DMS had begun. From the present perspective, the important implication is that J_i need not decrease rapidly with distance, contrary to the common belief among investigators of DMS.

Bruno and Lascaray[24] (BL) have suggested a much weaker distance dependence of the exchange constants J_2 to J_4 than that obtained from the detailed theory.[7,22,23] According to BL, J_2 should be a factor of 4 larger than J_4. Although the BL argument does not directly apply to the stannite structure, such an argument still suggests that J_2 should exceed J_4 by at least a factor of 2. This prediction is in disagreement with the result $|J_4|>|J_2/2|$ from the observed AF structure.

There is some evidence that even in some II-VI DMS's the exchange constant J_2 may not be larger than both J_3 and J_4. Recent magnetization-step data[25] suggest that in some Mn-based II-VI DMS, either J_3 or J_4 is larger than J_2. If these results are confirmed, then the present theory for the exchange interactions between distant neighbors in II-VI DMS will have to be modified.

More quantitative information about the exchange constants in Cu_2MnSnS_4 can be obtained using Θ and H_E. From Eq. (3), with $S=5/2$,

$$k_B\Theta=(70/3)(J_2+2J_3+J_4). \tag{4}$$

The *intersublattice* exchange field H_E is related to the exchange constants as

$$g\mu_BH_E=-2S\sum z_i'J_i, \tag{5}$$

where z_i' is the number of neighbors *on the opposite sublattice* which are coupled to a given Mn ion by the exchange constant J_i. For the present AF structure, $z_2'=2$, $z_3'=4$, and $z_4'=4$, so that

$$g\mu_BH_E=-10(J_2+2J_3+2J_4). \tag{6}$$

Using the experimental results for Θ and H_E, and setting $g=2.00$, one then obtains $J_4/k_B\cong-0.6$ K, and $(J_2+2J_3)/k_B\cong-0.5$ K.

Additional support for these values is obtained from the observed T_N. In mean-field theory for the present AF structure,

$$k_BT_N=-4J_4[2S(S+1)/3]. \tag{7}$$

Going beyond mean-field theory one typically has to multiply the right-hand side of Eq. (7) by a factor of about 0.7, assuming three-dimensional order.[18] From $T_N = 8.8$ K one then obtains $J_4/k_B \cong -0.5$ K, which is close to the estimate from Θ and H_E. The values for all the exchange constants in Cu_2MnSnS_4 are small compared to J_1 in II-VI DMS's, typically $J_1/k_B \cong -10$ K.[7,26] The weak exchange interactions in the stannite structure confirm the prediction of Wolff and Ram-Mohan[4] and Heiman *et al.*[5]

ACKNOWLEDGMENTS

The work at Tufts University was partially supported by NSF Grant No. DMR-9219727. The research in Zaragoza was supported by CICYT Grant No. MAT94-0043. The work at Brown University was supported by NSF Grant No. DMR-9221141. The Francis Bitter National Magnet Laboratory was supported by NSF. One of us (F.P.) has benefited from useful discussions with Jacques Schweizer, from CENG (Grenoble).

[1] *Semimagnetic Semiconductors and Diluted Magnetic Semiconductors*, edited by M. Averous and M. Balkanski (Plenum, New York, 1991).

[2] *Diluted Magnetic (Semimagnetic) Semiconductors*, edited by R. L. Aggarwal, J. K. Furdyna, and S. von Molnar, MRS Symposia Proceedings No. 89 (Materials Research Society, Pittsburgh, 1987).

[3] L. R. Ram-Mohan and P. A. Wolff, Phys. Rev. B **38**, 1330 (1988).

[4] P. A. Wolff and L. R. Ram-Mohan (Ref. 2), p. 1 ff.

[5] D. Heiman, E. D. Isaacs, P. Becla, and S. Foner (Ref. 2), p. 21 ff.

[6] L. Guen, W. S. Glaunsinger, and A. Wold, Mater. Res. Bull. **14**, 463 (1979).

[7] B. E. Larson, K. C. Hass, H. Ehrenreich, and A. E. Carlsson, Phys. Rev. B **37**, 4137 (1988).

[8] Y. Shapira, E. J. McNiff, Jr., N. F. Oliveira, Jr., E. D. Honig, K. Dwight, and A. Wold, Phys. Rev. B **37**, 411 (1988).

[9] J. Allemand and M. Wintenberger, Bull. Soc. Fr. Mineral. Cristallogr. **93**, 14 (1970).

[10] J. Allemand and M. Wintenberger, Bull. Soc. Fr. Mineral. Cristallogr. **93**, 141 (1970).

[11] G. H. McCabe, T. Fries, M. T. Liu, Y. Shapira, L. R. Ram-Mohan, C. Fau, M. Averous, R. Kershaw, A. Wold, and E. J. McNiff, Jr., Phys. Rev. B. (to be published).

[12] P. J. Brown and J. C. Matthewman, *The Cambridge Crystallographic Subroutine Library* (unpublished).

[13] M. S. Lehmann and F. K. Larsen, Acta Crystallogr. Sec. A **30**, 580 (1974).

[14] S. Foner, in *Magnetism*, edited by G. T. Rado and H. Suhl (Academic, New York, 1963), Vol. I, p. 383 ff.

[15] M. E. Fisher, Philos. Mag. **7**, 1731 (1962).

[16] Y. Shapira and S. Foner, Phys. Rev. B **1**, 3083 (1970); Y. Shapira, J. Appl. Phys. **42**, 1588 (1971).

[17] K. W. Blazey, H. Rohrer, and R. Webster, Phys. Rev. B **4**, 2287 (1971).

[18] L. J. de Jongh and A. R. Miedema, Adv. Phys. **23**, 1 (1974).

[19] H. Rohrer and H. Thomas, J. Appl. Phys. **40**, 1025 (1969).

[20] L. Corliss, N. Elliott, and J. Hastings, Phys. Rev. **104**, 924 (1956).

[21] D. Heiman, E. D. Isaacs, P. Becla, and S. Foner, Phys. Rev. B **35**, 3307 (1987).

[22] K. C. Hass, *Semimagnetic Semiconductors and Diluted Magnetic Semiconductors* (Ref. 1).

[23] T. M. Rusin, Phys. Rev. B **53**, 12 577 (1996).

[24] A. Bruno and J. P. Lascaray, Phys. Rev. B **38**, 9168 (1988).

[25] V. Bindilatti, N. F. Oliveira, Jr., E. ter Haar, and Y. Shapira, Czech. J. Phys. **46**, S6, 3255 (1996).

[26] Y. Shapira, J. Appl. Phys. **67**, 5090 (1990).